ACS APPLIED MATERIALS & INTERFACES

Research Article

www.acsami.org

Charge Transfer and Orbital Reconstruction in Strain-Engineered (La,Sr)MnO_3/$LaNiO_3$ Heterostructures

Jingjing Peng, Cheng Song,* Fan Li, Bin Cui, Haijun Mao, Yuyan Wang, Guangyue Wang, and Feng Pan*

Key Laboratory of Advanced Materials (MOE), School of Materials Science and Engineering, Tsinghua University, Beijing 100084, China

ABSTRACT: We investigate charge transfer, orbital reconstruction, and the emergence of exchange bias in (La,Sr)MnO_3/$LaNiO_3$ heterostructures. We demonstrate that charge transfer from Mn^{3+} ions to Ni^{3+} ions is accompanied by the formation of hybridized Mn/Ni $3z^2 - r^2$ orbits at the interface, instead of strain-stabilized Mn and Ni $x^2 - y^2$ orbits in the bulk films. In the heterostructures with ultrathin $LaNiO_3$, orbital reconstruction induced by charge transfer results in magnetization frustration of (La,Sr)MnO_3 at the interface. But the strain effect exerted by the growth of the $LaNiO_3$ top layer plays a dominant role on orbital reconstruction in the heterostructures with thick $LaNiO_3$, stabilizing $3z^2 - r^2$ orbits. In this case, robust spin glass, associated with larger magnetization frustration, accounts for the exchange bias effect. Our work builds a bridge between the microscopic electronic structure and the macroscopic magnetic property, providing the possibility of manipulating the exotic states with the aid of strain engineering in oxide-based electronics.

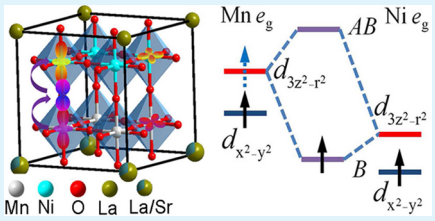

KEYWORDS: *charge transfer, orbital reconstruction, spin glass, strain effect, oxide-based electronics, exchange bias*

1. INTRODUCTION

Research in oxide interfaces, artificially constructed epitaxy heterostructures with atomic flatness, has flourished in the past decades due to a rich spectrum of exotic properties and unexpected states at the interface.[1−5] These properties are considered to be closely related to strong electronic correlations and intimate coupling between charge, spin, orbital, and lattice degrees of freedom, described by a simplified model involving charge transfer or orbital reconstruction.[3,6] These findings include the emergence of high-mobility conductivity at the classic $LaAlO_3$/$SrTiO_3$ interface due to the interface electronic reconstruction of the Ti 3d band[7,8] induced by charge transfer, orbital reconstruction in the interfacial CuO_2 layers at the $La_{0.67}Ca_{0.33}MnO_3$/(Y,Ca)-$Ba_2Cu_3O_7$ interface,[6,9] the unexpected ferromagnetic order arising in the Fe sublattice of $BiFeO_3$ at the $La_{0.7}Sr_{0.3}MnO_3$/$BiFeO_3$ interface,[10] and the orbital Ti ferromagnetism induced by charge transfer from Mn to Ti 3d band at the $LaMnO_3$/$SrTiO_3$ interface.[3] A minor variation of interfacial electronic state often causes a dramatic change of interfacial properties, and thus the understanding and manipulation of the electronic behavior would advance the use of interface in oxide-based electronics.[7,8,10−12]

Among oxide interfaces, heterostructures composed of magnetic materials offer an excellent illustration of the richness of interfacial phenomena and hold the potential for applications in spin valves, magnetic recording and reading heads.[2,13,14] The exchange bias, one of the outcomes of exchange anisotropy at the interface between a ferromagnetic (FM) and an antiferromagnetic (AFM) components, has also been discovered at the interface between ferromagnetic and paramagnetic (PM) oxide components in recent decades,[2,13−15] attracting a large amount of experimental and theoretical work to discern the nature of this interfacial exchange coupling. Though direct evidence of charge transfer can be obtained via element specific X-ray absorption spectroscopy (XAS) and X-ray magnetic circular dichroism (XMCD) measurements, there is still a lack of adequate information about orbital occupancy at the interface. Our work initiates the orbital degree of freedom in this system, which is remarkable in the field. On the other hand, the investigation of oxide interface has also triggered a renewed interest in manganites, where the mixture of Mn^{4+} (t_{2g}^3)/Mn^{3+} ($t_{2g}^3e_g^1$) of manganites leads to the double exchange that profoundly affects the electric and magnetic properties.[16−18] Here, we construct strain-engineered heterostructures consisting of ferromagnetic manganites and paramagnetic $LaNiO_3$ ($t_{2g}^6e_g^1$) to investigate whether a variation of electronic state has a fundamental influence on the orbital occupancy and the change of orbital occupancy would affect the interfacial properties. It is especially noted that epitaxial strain from the substrate plays a dominate role in manipulating the orbital occupancy, however, the question remains unexplored whether the strain from top layer will have an effect on the orbital occupancy, which is novel in this field. Our strain-engineered heterostructures provide such an opportunity to dwell on the issue, the results of which indicate the importance of the strain introduced by top layer in the manipulation of orbital occupancy. On the other hand, the experiments below not only focus on the verification of charge transfer, orbital reconstruction and spin glass (SG) related exchange bias at

Received: April 18, 2015
Accepted: July 27, 2015
Published: July 27, 2015

DOI: 10.1021/acsami.5b04994
ACS Appl. Mater. Interfaces 2015, 7, 17700−17706

the ferromagnet/paramagnet (La,Sr)MnO_3/$LaNiO_3$ (LSMO/LNO) interface, but also tend to build the intrinsic correlation among them, thus providing the possibility of manipulating and benefiting from exotic states in oxide-based electronics.

2. EXPERIMENTAL SECTION

LSMO/LNO(t) bilayers were prepared by initially growing 24 u.c. LSMO from a stoichiometric $La_{0.67}Sr_{0.33}MnO_3$ target on atomically flat $SrTiO_3$ (001) substrates and then depositing t u.c. LNO overlayer on top, where t ranges from 0, 4, 8, 12, 16, 24, 36, 72 u.c. All of the films were grown by pulsed laser deposition (PLD) at 700 °C and under an oxygen pressure of 20 mTorr to avoid any change of oxygen vacancies density at the interface. The layer-by-layer growth mode is identified by reflection high-energy electron diffraction (RHEED), which enables precise calculation of film thickness at the atomic level. The samples were cooled to room temperature under 500 Torr oxygen pressure to further avoid oxygen vacancies. Mn L-edge XAS and X-ray linear dichroism (XLD) measurements were performed ex situ at Beamline BL08U1A of the Shanghai Synchrotron Radiation Facility (SSRF) in total electron yield (TEY) mode at room temperature. The background vacuum level was 8×10^{-7} Torr. The energy scale was calibrated via the known peak position of the MnO_2 test sample, which was measured in the same condition as that of the bilayers. The spectra normalization was made through dividing the spectra by a factor so that the L_3 pre-edge and L_2 postedge have identical intensities for the two polarizations.[19] After that, the spectra were normalized to the maximum of L_3 edge. XLD, the difference between the XAS in-plane ($E//a$) and out-of-plane ($E//c$) components, gives direct insight of the preferential orbital occupancy. The magnetization measurements were performed by superconducting quantum interference device (SQUID) magnetometry with the magnetic field (H) applied in-plane along the (100) direction of the substrate with a size of 5 mm × 5 mm. All the $M-H$ (magnetization versus magnetic field) measurements in this work without a special statement were performed after cooling from room temperature to 5 K in zero-field-cooled (ZFC) or field-cooled (FC) processes, during which the cooling field was +0.5 kOe. All the $M-T$ (magnetization versus temperature) measurements were measured during the warming process after cooling from room temperature to 5 K in ZFC or FC processes, during which the cooling field was +0.5 kOe. The hysteresis curves were obtained after subtracting the diamagnetic background due to the diamagnetic susceptibility of the substrate.

3. RESULTS AND DISCUSSION

XAS is utilized to detect the electronic structure near the interface, taking advantage of the element specificity and shallow probing depth of several nanometers in TEY mode.[20] In Figure 1a, we first show Mn L-edge XAS of the LSMO/LNO, where the thickness of the LSMO bottom layer is fixed at 24 unit cell (u.c.), while the LNO thickness (t) varies from 0 to 16 u.c. for a series of samples. In this experiment the Mn valence states in the vicinity of the LSMO/LNO interface are mainly probed in the samples with relatively thick LNO. The XAS at Mn L-edge is sensitive to Mn $2p_{3/2,1/2} \rightarrow 3d$ dipole transitions, providing information on the unoccupied Mn 3d state and related Mn valence.[20,21] Separated by the spin−orbit splitting of the Mn 2p core hole, the spectra exhibit two broad multiplets generally defined as Mn L_3 and L_2 peak, respectively. The most striking result here is the shift of L_3 peak toward high energy direction upon increasing the LNO thickness, indicating the increase of Mn valence states when approaching the LSMO/LNO interface. This can be attributed to the existence of the LNO overlayer directly adjacent to it. It should be mentioned that the decreased signal-to-noise ratio of the spectra in the samples with thicker LNO reflects the shallow probing depth of XAS.[20]

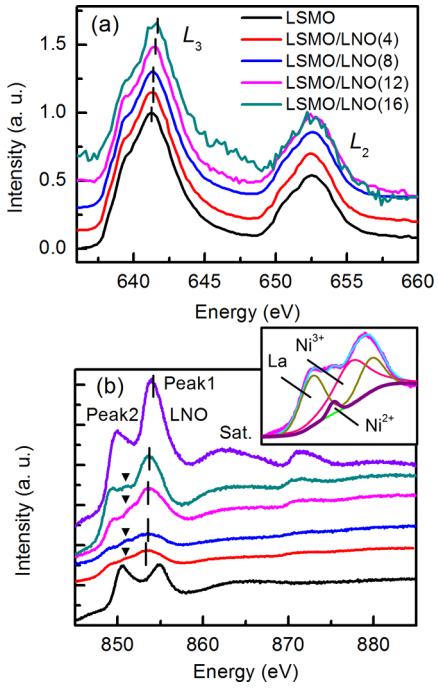

Figure 1. (a) Mn L edge XAS curves of LSMO/LNO(t) bilayers on $SrTiO_3$ substrates, with LNO thickness t being 0, 4, 8, 12, and 16 u.c., respectively. The two broad multiplets of the Mn L-edge are denoted as L_3 and L_2. (b) Ni 2p XPS spectra of bilayers LSM/LNO with LNO overlayer thickness t being 0, 4, 8, 12, and 16 u.c. as well as 24 u.c. LNO single film directly grown on $SrTiO_3$ substrates. Peak 1 is composed of Ni 2p 3/2 and the satellite peak of La 3d 3/2. Sat. denotes the satellite peaks of Ni 2p XPS spectra and the arrows identify the location of the third peak between peak 1 and peak 2. The inset shows multiple-peak fittings for the Ni 2p core-level spectra in the energy range of 845−858 eV for the bilayer LSMO/LNO(16). The proportion of the Ni^{2+} /(Ni^{2+}/Ni^{3+}) in the samples could then be estimated by the areas under the Ni^{2+} (thick solid line) and Ni^{3+} peaks.

Since La M_4 and Ni L_3 edge overlap to some extent, X-ray photoelectron spectroscopy (XPS) instead of XAS was utilized for the characterization of Ni chemical information as shown in Figure 1b, taking advantage of the extra information provided by the satellite peaks. A direct measurement of Ni valence states close to the interface can be obtained with the XPS spectra of those with thinner LNO overlayer. Peak 1 around 854 eV is composed of Ni 2p 3/2 peak and the satellite peak of La 3d 3/2. Given that the contribution from La 3d 3/2 peaks is almost constant in all the spectra,[22] the shift of peak 1 toward lower energy direction upon decreasing the LNO thickness gives a hint about the lower Ni valence states at the interface. Meanwhile, the spectra of the bilayers differ from that of LNO or LSMO single films and the line shape of the Ni 2p XPS spectra changes notably with different thicknesses of the LNO overlayer. The appearance of a third peak between peak 1 and peak 2 marked by arrows is clearly recognizable on decreasing the LNO thickness, which is quite characteristic of the XPS spectra of NiO.[23] As the formation of NiO can be ruled out by high resolution transmission electron microscope (not shown here), the appearance of NiO like peak only manifests a reduction of valence states or a tendency toward Ni^{2+} for the interfacial Ni^{3+}. Recalling the increase of Mn valence at the interface as proved by Mn L-edge XAS, it is quite natural to consider a charge transfer from Mn ions to Ni ions at the LSMO/LNO interface. We note that charge transfer takes place

DOI: 10.1021/acsami.5b04994
ACS Appl. Mater. Interfaces 2015, 7, 17700−17706

at the interface despite the thickness of LNO, which can be understood by taking into account that LSMO is half metal and deterioration of conductivity of LNO would not destroy the interfacial coupling.

Mn L-edge XLD, the difference between the XAS in-plane (E//a) and out-of-plane (E//c) components, namely $I_{ab} - I_c$, was employed to elucidate the occupancy of Mn 3d orbits. Long time exposure of samples to the x−ray beam may induce some unexpected modifications of the spectra around the L_3 peak, which can lead to erroneous determination of the XLD signal.[19] Therefore, we chose the method of the integration around the L_2 peak (647.5−660.0 eV). And the area under XLD around the L_2 peak (A_{XLD}) represents the difference between the relative occupancies of the $3z^2 - r^2$ and $x^2 - y^2$ orbits.[16,19] A positive (negative) A_{XLD} on average is due to a preferential occupancy of the out-of-plane $3z^2 - r^2$ (in-plane $x^2 - y^2$) orbits. Any contribution to the XLD data from the magnetization discrepancy of the samples ought to be of little influence, because the magnetization is weak at this temperature (300 K), and the small magnetic signals could not fundamentally change the orbital occupany.[24,25] The difference spectra as well as the in-plane and out-of-plane spectra are depicted in Figure 2. As expected, the single LSMO film has a negative A_{XLD} (Figure 2a), elucidating that $x^2 - y^2$ orbits rather than $3z^2 - r^2$ orbits are energetically preferred for LSMO films with tensile strain from $SrTiO_3$ substrates.[19,26] For the LSMO/LNO samples with the 4 u.c. and 8 u.c. LNO layer on top, the A_{XLD} is less negative, compared with that in Figure 2a. As there is still a large contribution from the bulk LSMO, the A_{XLD} is still

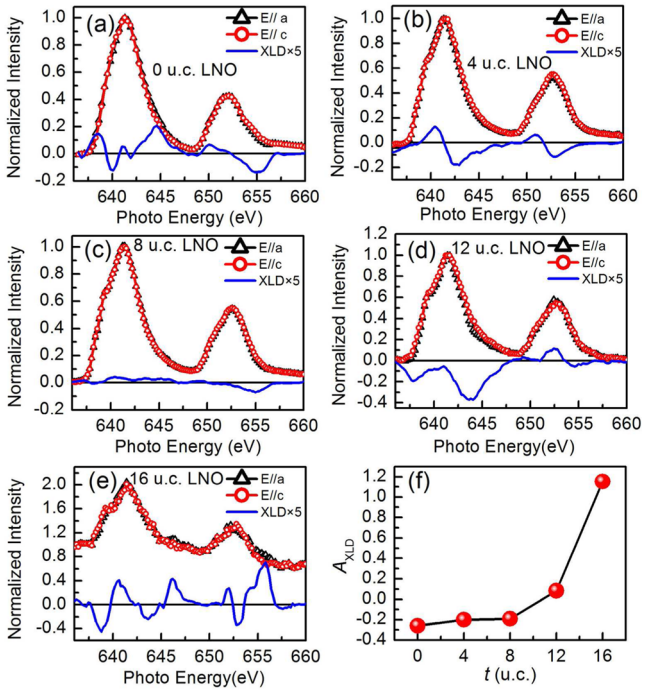

Figure 2. Normalized XAS and XLD of LSMO/LNO(t) bilayers on STO substrates, with LNO thickness t being 0 u. c. (a), 4 u. c. (b), 8 u. c. (c), 12 u.c. (d), and 16 u.c. (e), while the thickness of the LSMO bottom layer is fixed at 24 u.c. Mn L edge XLD, the difference between the XAS in-plane and out-of-plane components, namely $I_{ab} - I_c$, elucidates the occupancy of Mn 3d orbits. The area under XLD around the L_2 peak (647.5−660.0 eV) (A_{XLD}) represents the difference between the relative occupancies of the $3z^2 - r^2$ and $x^2 - y^2$ orbits. A summary of A_{XLD} (XLD × 5) for different bilayers is plotted in (f).

negative. We can also conclude that orbital reconstruction takes place at the interface despite the thickness of LNO, in accordance with charge transfer effect. For t = 12 u.c., a positive value of A_{XLD} emerges in Figure 2d, revealing a preferential orbital occupancy of $3z^2 - r^2$ orbits, which essentially differs from that without LNO. The trend is even more pronounced by increasing the LNO thickness to 16 u.c. (Figure 2e), but along with a worse signal-to-noise ratio as a result of the shallow probing depth of TEY mode. Given that there is not much difference in interfacial properties among those bilayers (as will be discussed in Figure 4a), XLD is capable to detect more information closer to the interface by increasing the thickness of LNO top layer. A summary of A_{XLD} for different bilayers plotted in Figure 2f indicates an increasing trend of $3z^2 - r^2$ orbits occupancy toward the interface, in close analogy to an increase of Mn valence states and a decrease of Ni valence states at the interface namely charge transfer. In this case, the positive A_{XLD}, i.e., a preferential orbital occupancy of $3z^2 - r^2$, suggests that the interfacial LSMO favors Mn $3z^2 - r^2$ orbits in vast contrast with the "bulk" preferential $x^2 - y^2$ orbits, referred to as interfacial orbital reconstruction. Similar results about a prominent $3z^2 - r^2$ orbit occupancy is reported at the free surface of LSMO thin films owing to surface symmetry-breaking.[19] For LSMO/LNO interface, the preferred $3z^2 - r^2$ orbits occupancy for interfacial LSMO must be closely related to the LNO directly adjacent to it, since charge transfer effect may result in interfacial coupling and thus greatly affect the orbital occupancy.[3,16]

We then describe a possible microscopic scenario for the correlation between charge transfer and orbital reconstruction. Figure 3a shows a schematic of the interface between LSMO and LNO where the hybridization of $3z^2 - r^2$ orbits results in strong interfacial coupling and no hybridization of $x^2 - y^2$ orbits is suggested to occur due to the slight overlap of electron cloud. Before taking into account the hybridization, the prerequisite of the Fermi energy continuity suggests the possible energy alignment as shown in the left and right column of Figure 3b in which the energy level of Ni ions is lower than that of Mn owing to the metallic nature of LNO and half-metallic nature of LSMO. The Ni^{3+} and Mn^{3+} ions possess electronic configurations of low spin $t_{2g}^6e_g^1$ and high spin $t_{2g}^3e_g^1$ states, respectively.[27,28] Spin−orbit coupling is a mechanism by which spins feel the distribution of the electronic density (orbits) and is described by a Hamiltonian of the form $H_{SO} = \lambda$ L·S, where L is the orbital angular momentum and S is the spin angular momentum. And for symmetry reasons, the matrix elements of the orbital momentum operator functioning on e_g states are zero; thus, we have tentatively omitted the effect of spin−orbit coupling in our system.[3]

When it comes to interfacial orbit hybridization, the orbital occupancy of LSMO and LNO before hybridization is another crucial factor. For LNO, the planar $x^2 - y^2$ orbital order is driven by the reduced dimensionality and epitaxial strain from the LSMO layer.[29,30] For LSMO, the preferential occupancy of $x^2 - y^2$ orbits is due to the substrate strain, which lifts the energy level of the $3z^2 - r^2$ orbits. At the interface, strong hybridization between Mn $3z^2 - r^2$ band and the empty $3z^2 - r^2$ band of Ni at the interface would form the bonding (B) $3z^2 - r^2$ orbits and antibonding (AB) $3z^2 - r^2$ orbits. That is, extended molecular orbits consist of atomic Mn and Ni $3z^2 - r^2$ orbits with an admixture of the p_z orbits on the apical oxygen (Figure 3a). The hybridization of the Mn $x^2 - y^2$ orbits and Ni orbits as well as hybridization of t_{2g} bands of Ni and Mn across

DOI: 10.1021/acsami.5b04994
ACS Appl. Mater. Interfaces 2015, 7, 17700−17706

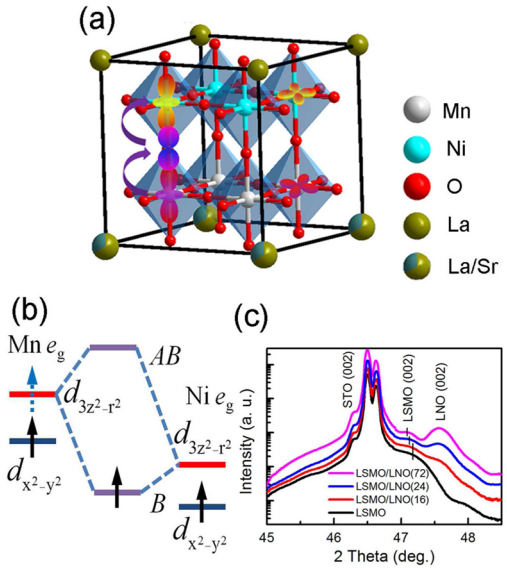

Figure 3. (a) Schematic of the interface between LSMO and LNO where the hybridization of $3z^2 - r^2$ orbits results in strong interfacial coupling and no hybridization of $x^2 - y^2$ orbits is suggested to occur due to little overlap of electron cloud. The overlap between the O p_z orbit and adjacent Mn and Ni $3z^2 - r^2$ orbits results in strong hybridization and the formation of extended molecular orbits, which is a high mobility passageway for charge transfer from Mn to Ni. (b) Schematic of orbital reconstruction and the formation of molecular orbits between interfacial Mn and Ni occupying strain stabilized $x^2 - y^2$ orbits. The dotted arrow represents an intermediate state of Mn electron occupying Mn $3z^2 - r^2$ orbits. AB and B refer to antibonding and bonding, respectively. (c) XRD spectra of LSMO single layer and LSMO/LNO bilayers with t being 16, 24, and 72 u.c.

the interface is negligibly small due to the weak coupling strength between them.[10,14] After hybridization, the electrons would take the lowest energy level, e.g., the bonding $3z^2 - r^2$ orbits. In this scenario, the electrons are transferred from the Mn $x^2 - y^2$ orbits to an intermediate state of Mn $3z^2 - r^2$ orbits, and then finally to the molecular $3z^2 - r^2$ orbits shared by Mn and Ni at the interface, as sketched in Figure 3b. As for the split between the Mn^{4+}/Mn^{3+} and Ni^{3+}/Ni^{2+} redox couples, it takes an energy of 0.85 eV to transfer an electron from a Ni^{2+} to a Mn^{4+},[31,32] namely the Fermi level of LNO is aligned below the Fermi level of LSMO that allows charge transfer to occur. This scenario could successfully explain the observed preferential occupancy of $3z^2 - r^2$ orbits.

The experiment above confirms that charge transfer leads to orbital reconstruction at the interface for the heterostructures with ultrathin LNO. Note that the LNO has a smaller bulk lattice parameter (0.384 nm) than LSMO (0.387 m), thus with increasing film thickness, the LNO overlayer is expected to introduce the strain effect to the LSMO layer, especially taking by increasing strain driven by LNO we can detect whether orbital occupancy can be further controlled by strain in this heterostructures. As indicated by XRD spectra shown in Figure 3c, there is no shift of LSMO (002) peak for t less than 16 u.c., which indicates that orbital reconstruction induced by charge transfer as proved above is mainly located at the interface. However, further increasing t from 24 to 72 u.c., we find an increasing shift of LSMO (002) peak toward a smaller angle, indicating that the strain effect introduced by the deposition of LNO top layer causes the elongation of the out-of-plane lattice parameters. It is natural to take into account the fact that the epitaxial strain from the STO substrate plays a dominant role in determining the in-plane lattice parameter of the bilayer.[33] Then it is expected that a variation of out-of-plane lattice parameter may be a reflection of the strain effect. The elongation of the out-of-plane lattice parameters would stabilize the preferred $3z^2 - r^2$ orbit occupancy.[34−36] Thus, it is concluded that the strain exerted by a comparatively thick LNO overlayer leads to orbital reconstruction.

We now focus on examining the effect of charge transfer and orbital reconstruction on the macroscopic magnetic property of the LSMO/LNO bilayers. Figure 4a shows hysteresis loops of

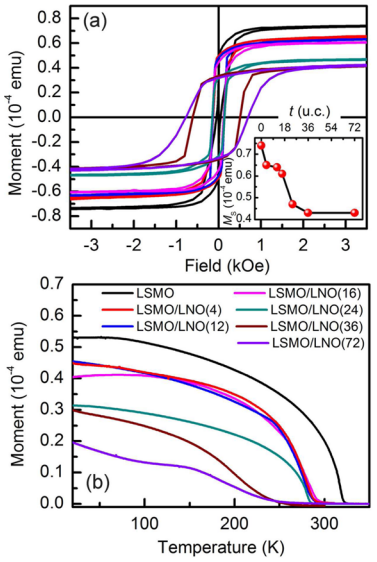

Figure 4. (a) $M-H$ loops of the bilayers with LSMO/LNO(t) bilayers with LNO thickness t being 0, 4, 12, 16, 24, 36, and 72 u.c., measured at 5 K after +0.5 kOe field cooling from room temperature. The t dependent M_S is plotted in the inset. (b) $M-T$ curves of the bilayers with LSMO/LNO bilayers with LNO thickness t being 0, 4, 12, 16, 24, 36, and 72 u.c.

the bilayers as the LNO changing from 0 to 72 u.c., while the LSMO remains at 24 u.c. The hysteresis loops were obtained at 5 K after a field-cooling procedure from room temperature in a + 0.5 kOe field. The most striking feature here is the step-like depression of saturated magnetization (M_S; in the inset of Figure 4a) upon increasing LNO thickness, which is indeed surprising, because the LSMO film thickness is constant and paramagnetic LNO contributes very little to the overall ferromagnetism. The depression remains almost constant (14%) when LNO thickness is less than 16 u.c.. It is confirmed by the temperature dependent magnetization ($M-T$) curves presented in Figure 4b with an apparently reduced magnetic moment and Curie temperature (T_C) observed in bilayers with LNO. The LSMO film without LNO exhibits a T_C of 323 K lower than the bulk value of 370 K, which is quite normal for the ultrathin LSMO films,[37] while the bilayers with 4, 12, and 16 u. c. LNO exhibits a much lower T_C of 285 K. The depressed M_S and the reduced T_C, referred to as magnetization frustration, indicate that the LNO overlayer profoundly affects the magnetic behavior of the LSMO film. Based on the scenario described above, the preferential $3z^2 - r^2$ orbits occupancy at the interface tends to reduce the double exchange mechanism, resulting in C-type antiferromagnetism. In other words, the anisotropy of d orbits affects the electron correlation effects in an orbital direction dependent manner, thus yield the

DOI: 10.1021/acsami.5b04994
ACS Appl. Mater. Interfaces 2015, 7, 17700−17706

anisotropy of the electron transfer and eventually destroy the double exchange order, leading to the suppressed magnetization.[26] To verify this scenario, we have made estimation of the transferred charge at this interface combined with the Mn *L*-edge XAS and Ni 2p XPS in Figure 1. The Mn *L*-edge XAS of the bilayer with 16 u.c. LNO mainly reflects the valence state of interfacial Mn, which shows a shift of 0.38 eV compared with that of bare LSMO, corresponding to 0.25 electron per Mn atom. The LSMO/LNO(16) sample exhibits ~14% magnetization depression, for which 3.3 u.c. LSMO is involved, in the scale of the screening length for manganites.[38] Subsequently, approximately 0.83 electrons are transferred, resulting in 5.2% Ni^{2+} in the 16 u.c. LNO layer, which is in agreement with the fitted value of 5.8% Ni^{2+} based on multiple-peak fittings of Ni 2p XPS, as presented in the inset of Figure 1b. Similar estimation can be done in the bilayers with 12 and 8 u.c. LNO. It is worthy pointing out that the transferred electrons enter p-type conductive LNO,[39] possibly causing the transition of the interfacial LNO from metal to insulator, where Ni^{2+} is preferred to exist compared to the bulk.

On the other hand, further increasing LNO thickness from 16 u.c. to 72 u.c., we obtain the largest depression of M_S up to ~40% and a reduced T_C to 250 K. That is to say further increase of LNO thickness would introduce another important factor that would cause magnetization frustration in addition to orbital reconstruction caused by the interfacial charge transfer effect. This is the strain effect as mentioned above. For the bilayers with thicker LNO ($t \geq 16$ u.c.), the compressive strain exerted by the comparatively thick LNO overlayer advances a preferential occupancy of the out-of-plane $3z^2 - r^2$ orbit,[11] probably enhancing orbital reconstruction deep into the LSMO layer. This means that around 10 u.c. of LSMO is influenced by orbital reconstruction, comparable to the thickness of interfacial dead layer of LSMO grown on $LaAlO_3$ substrates with compressive strain.[16] The step-like depression of magnetization clearly indicates that there are two competing factors: the interfacial charge transfer induced orbital reconstruction, and the strain effect induced orbital reconstruction much deeper into the LSMO.

Another notable feature of Figure 4a is the appearance of exchange bias (EB) behavior of the bilayers. A shift of the hysteresis loops to the negative field direction after cooling down in +0.5 kOe field gives rise to the exchange bias field $|H_{EB}|$ of ~54 Oe for $t \geq 36$ u.c.. Upon cooling in a magnetic field with the opposite sign, e.g., − 0.5 kOe, the loop shifts to the positive field direction (not shown here), which verifies the EB behavior. Besides, the apparent increase of the coercive field is observed in the bilayers with thicker LNO, which can be explained by the introduction of the EB.[40] To trace the origin of the EB behavior in the nominal ferromagnet/paramagnet LSMO/LNO system, hysteresis loops of bilayers with 36 u.c. LNO were selectively measured at 5 K after cooling from room temperature under different magnetic fields H_{FC} of 0.1, 0.3, 0.5, 2, 10, and 50 kOe. Corresponding data are shown in Figure 5a. All the hysteresis loops show the same M_S but with distinct coercivities, especially on the descending branch. Subsequently, H_{FC} dependent H_{EB} is summarized in Figure 5b. We note that H_{EB} increases rapidly to 54 Oe as H_{FC} = 0.5 kOe, and then decreases monotonously to zero after cooling in a high field of 50 kOe, which is quite characteristic of the exchange bias effect involving SG state rather than antiferromagnetic/ferromagnetic systems.[37,41] First, the H_{FC} about 0.5 kOe which forces the maximum H_{EB} is much lower than that of AF/FM systems but

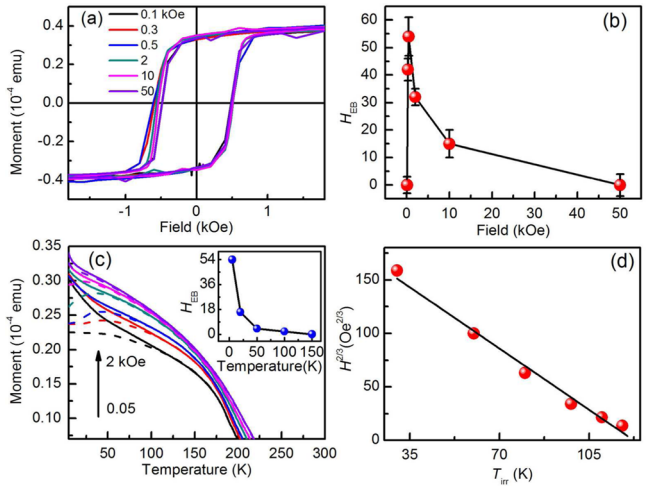

Figure 5. (a) *M*−*H* loops of the bilayers with 36 u.c. LNO were measured 5 K after cooling from room temperature under a magnetic field H_{FC} of 0.1, 0.3, 0.5, 2, 10, and 50 kOe. (b) H_{EB} as a function of H_{FC}. (c) *M*−*T* curves measured under various fields (H = 0.05, 0.1, 0.2, 0.5, 1, and 2 kOe). The solid and dashed lines are the FC and ZFC data, respectively. The T dependent H_{EB} is plotted in the inset. (d) The corresponding plot of $H^{2/3}$ vs T_{irr} and linear fitting to eq 1 are shown in the inset. The magnetization measurements were made by applying in-plane magnetic field (H) along the (100) direction of the samples.

approaches that of the SG-based EB system. Second, there is a sudden drop of H_{EB} upon increasing H_{FC} in vast contrast to a saturation of maximum H_{EB} value at a much higher H_{FC} for AF/FM systems.[21,42] Thus, it can be derived that the exchange bias is not caused by LSMO pinned by the interfacial NiO.

In order to further confirm the existence of the SG state at the LSMO/LNO interface, *M*−*T* curves under different fields of 0.05, 0.1, 0.2, 0.5, 1, and 2 kOe after field-cooled (FC) and zero-field-cooled (ZFC) processes were measured. Concomitant data are depicted in Figure 5c. There are two main features for the curves: a peak in the ZFC *M*-*T* curves (T_{peak}) and a bifurcation between the ZFC and FC curves below the irreversibility temperature T_{irr}, which is frequently observed in a SG-based EB system.[37] Furthermore, the two characteristic temperatures are quite close, especially at a lower measurement field, and upon increasing measurement field both temperatures are greatly reduced, which is characteristic of the SG behavior and suggests that the frozen SG state is clearly suppressed by a strong magnetic field.[41] As illustrated in Figure 5d, the SG nature of the bilayer is reconfirmed by the measurement field dependent T_{irr} following the Almeida−Thouless line,[43] which is given by

$$H(T_{irr})/\Delta J \propto (1 - T_{irr}/T_F)^{3/2} \quad (1)$$

where T_F is the zero-field SG freezing temperature and ΔJ is the width of the distribution of the exchange interaction. The linear fit of the Almeida−Thouless line in Figure 5d bolsters the existence of the SG behavior in LSMO with a freezing temperature $T_F \approx 122$ K, given by the extrapolation of the Almeida−Thouless line back to zero field. The temperature dependent H_{EB} of LSMO/LNO(36) is depicted in the inset of Figure 5c, which shows a blocking temperature (T_B) of about 100 K, close to the T_F. This suggests that the competition of the magnetic orders and the emergence of the SG state play important roles in the EB effect.[41] Without low-temperature Ni

DOI: 10.1021/acsami.5b04994
ACS Appl. Mater. Interfaces 2015, 7, 17700−17706

XMCD, we cannot fully exclude the existence of induced Ni ferromagnetism. Nevertheless, the exchange bias in similar system[14,15] is not attributed to interfacial Ni magnetism, since the effective exchange coupling across the LSMO/LNO interface, $|J_{LSMO-LNO}|$, is weaker than the other coupling mechanism in the samples: $|J_{Ni-Ni}|$ and $|J_{Mn-Mn}|$,[14] and thus the exchange bias results from LSMO pinned by the competition of magnetic interactions induced magnetic frustrated states, which are usually of SG nature.

So far, we have confirmed the existence of SG at the LSMO/LNO, which usually originates from the competition between the AFM and FM interaction in most systems.[18,26] Recalling the orbital reconstruction, the stabilization of $3z^2 - r^2$ orbits for the interfacial LSMO tends to reduce the in-plane double exchange, and instead *C*-type AFM structure is favored. Thus, the long-range FM order is disturbed by the *C*-type AFM structure, which not only causes the magnetization suppression as mentioned above but also breeds the interfacial SG.[41] The spins in the SG regions partly frozen collinearly with the field direction serve as the uncompensated spins and induce the EB effect. What further intrigues us is that the exchange bias is absent in the bilayers with LNO thickness less than 36 u.c. while the coercivity enhancement is still present. Both exchange bias and the coercivity enhancement originate from the exchange coupling at the interface, but the coercivity enhancement can be recognized as long as there is exchange coupling, and the exchange bias only shows up when there is enough antiferromagnetic moment or SG to pin the ferromagnetic part. In the sample with thicker LNO, we see much more depression of magnetization (shown in Figure 4a), which may indicate that there is more intensive exchange coupling or more robust SG at the interface. This is because the increase of the LNO thickness has a strengthened strain on LSMO and stabilizes preferential $3z^2 - r^2$ orbits occupancy. Enhanced preferential orbital occupancy would further disturb the double exchange ferromagnetic order inside the LSMO and thus robust SG state comes into being to pin the bulk ferromagnetic LSMO, guaranteeing the exchange bias behavior. Another factor to be considered here is how much this exchange bias and the depression of M_S are affected by the interdiffusion, which may be minor but cannot be fully excluded. Note that a transition from a ferromagnetic to an antiferromagnetic state in LSMO needs a variation of Sr content of ∼17% with respect to the phase diagram,[17] and an antiferromagnetic behavior can only be expected in $LaNiO_{2.5}$.[44]

4. CONCLUSIONS

To summarize, the LSMO/LNO interface displays orbital reconstruction induced magnetization frustration, namely a preferential orbital occupancy of $3z^2 - r^2$ caused by charge transfer from Mn^{3+} to Ni^{3+} ions with the formation of hybridized Mn/Ni $3z^2 - r^2$ orbits at the interface. Furthermore, this orbital reconstruction can be further enhanced by the strain effect from top LNO layer, leading to larger magnetization frustration and the intriguing exchange bias effect at the interface. We confirm that the exchange bias is intimately correlated to the formation of a robust SG state brought by the competition of magnetic interactions which induced magnetic frustrated states near the interface. The accomplishment of this work can be readily generalized to other oxide heterostructures and thus offers a broad opportunity to tailor and benefit from the exotic states in strain-engineered heterostructures.

AUTHOR INFORMATION

Corresponding Authors

*E-mail: songcheng@mail.tsinghua.edu.cn.
*E-mail: panf@mail.tsinghua.edu.cn.

Notes

The authors declare no competing financial interest.

ACKNOWLEDGMENTS

The authors acknowledge Beamline BL08U1A in Shanghai Synchrotron Radiation Facility (SSRF) for XAS and XLD measurements. This work was supported by the National Natural Science Foundation of China (Grant Nos. 51322101, 51202125 and 51231004) and National Hi-tech (R&D) project of China (Grant Nos. 2014AA032901 and 2014AA032904).

REFERENCES

(1) Hwang, H. Y.; Iwasa, Y.; Kawasaki, M.; Keimer, B.; Nagaosa, N.; Tokura, Y. Emergent Phenomena at Oxide Interfaces. *Nat. Mater.* **2012**, *11*, 103−113.

(2) Gibert, M.; Zubko, P.; Scherwitzl, R.; Íñiguez, J.; Triscone, J. M. Exchange Bias in $LaNiO_3$-$LaMnO_3$ Superlattices. *Nat. Mater.* **2012**, *11*, 195−198.

(3) Garcia-Barriocanal, J.; Cezar, J. C.; Bruno, F. Y.; Thakur, P.; Brookes, N. B.; Utfeld, C.; Rivera-Calzada, A.; Giblin, S. R.; Taylor, J. W.; Duffy, J. A. Spin and Orbital Ti Magnetism at $LaMnO_3$/$SrTiO_3$ Interfaces. *Nat. Commun.* **2010**, *1*, 82.

(4) Zubko, P.; Gariglio, S.; Gabay, M.; Ghosez, P.; Triscone, J. M. Interface Physics in Complex Oxide Heterostructures. *Annu. Rev. Condens. Matter Phys.* **2011**, *2*, 141−165.

(5) Cheng, Z. X.; Hong, F.; Wang, Y. X.; Ozawa, K.; Fujii, H.; Kimura, H.; Du, Y.; Wang, X. L.; Dou, S. X. Interface Strain-Induced Multiferroicity in a $SmFeO_3$ Film. *ACS Appl. Mater. Interfaces* **2014**, *6*, 7356−7362.

(6) Satapathy, D.; Uribe-Laverde, M.; Marozau, I.; Malik, V.; Das, S.; Wagner, T.; Marcelot, C.; Stahn, J.; Brück, S.; Rühm, A. Magnetic Proximity Effect in $YBa_2Cu_3O_7$/$La_{2/3}Ca_{1/3}MnO_3$ and $YBa_2Cu_3O_7$/$LaMnO_{3+\delta}$ Superlattices. *Phys. Rev. Lett.* **2012**, *108*, 197201.

(7) Ohtomo, A.; Hwang, H. Y. A High-mobility Electron Gas at the $LaAlO_3$/$SrTiO_3$ Heterointerface. *Nature* **2004**, *427*, 423−426.

(8) Lee, J.-S.; Xie, Y.; Sato, H.; Bell, C.; Hikita, Y.; Hwang, H.; Kao, C.-C. Titanium dxy Ferromagnetism at the $LaAlO_3$/$SrTiO_3$ Interface. *Nat. Mater.* **2013**, *12*, 703−706.

(9) Chakhalian, J. K.; Freeland, J. W.; Srajer, G.; Strempfer, J.; Khaliullin, G.; Cezar, J. C.; Charlton, T.; Dalgliesh, R.; Bernhard, C. H.; Cristiani, G. Magnetism at the Interface between Ferromagnetic and Superconducting Oxides. *Nat. Phys.* **2006**, *2*, 244−248.

(10) Yu, P.; Lee, J. S.; Okamoto, S.; Rossell, M. D.; Huijben, M.; Yang, C. H.; He, Q.; Zhang, J. X.; Yang, S. Y.; Lee, M. J. Interface Ferromagnetism and Orbital Reconstruction in $BiFeO_3$-$La_{0.7}Sr_{0.3}MnO_3$ Heterostructures. *Phys. Rev. Lett.* **2010**, *105*, 027201.

(11) Pan, F.; Gao, S.; Chen, C.; Song, C.; Zeng, F. Recent Progress in Resistive Random Access Memories: Materials, Switching Mechanisms, and Performance. *Mater. Sci. Eng., R* **2014**, *83*, 1−59.

(12) Mathew, S.; Annadi, A.; Chan, T. K.; Asmara, T. C.; Zhan, D.; Wang, X. R.; Azimi, S.; Shen, Z.; Rusydi, A.; Ariando; Breese, M. B. H.; Venkatesan, T. Tuning the Interface Conductivity of $LaAlO_3$/$SrTiO_3$ Using Ion Beams: Implications for Patterning. *ACS Nano* **2013**, *7*, 10572−10581.

(13) Dong, S.; Dagotto, E. Quantum Confinement Induced Magnetism in $LaNiO_3$-$LaMnO_3$ superlattices. *Phys. Rev. B: Condens. Matter Mater. Phys.* **2013**, *87*, 195116.

(14) Sánchez, J. R.; Nelson-Cheeseman, B.; Granada, M.; Arenholz, E.; Steren, L. B. Exchange-bias Effect at $La_{0.75}Sr_{0.25}MnO_3$/$LaNiO_3$ Interfaces. *Phys. Rev. B: Condens. Matter Mater. Phys.* **2012**, *85*, 094427.

(15) Hoffman, J.; Tung, I. C.; Nelson-Cheeseman, B. B.; Liu, M.; Freeland, J. W.; Bhattacharya, A. Charge Transfer and Interfacial

DOI: 10.1021/acsami.5b04994
ACS Appl. Mater. Interfaces 2015, 7, 17700−17706

Magnetism in $(LaNiO_3)n/(LaMnO_3)_2$ Superlattices. *Phys. Rev. B: Condens. Matter Mater. Phys.* **2013**, *88*, 144411.
(16) Cui, B.; Song, C.; Li, F.; Wang, G. Y.; Mao, H. J.; Peng, J. J.; Zeng, F.; Pan, F. Tuning the Entanglement between Orbital Reconstruction and Charge Transfer at a Film Surface. *Sci. Rep.* **2014**, *4*, 4206.
(17) Cui, B.; Song, C.; Yan, Y. N.; Miao, J. H.; Zeng, F.; Pan, F. Reversible Ferromagnetic Phase Transition in Electrode-Gated Manganites. *Adv. Funct. Mater.* **2014**, *24*, 7233−7240.
(18) Cui, B.; Song, C.; Gehring, G. A.; Li, F.; Wang, G. Y.; Chen, C.; Peng, J. J.; Mao, H. J.; Zeng, F.; Pan, F. Electrical Manipulation of Orbital Occupancy and Magnetic Anisotropy in Manganites. *Adv. Funct. Mater.* **2015**, *25*, 864−870.
(19) Pesquera, D.; Herranz, G.; Barla, A.; Pellegrin, E.; Bondino, F.; Magnano, E.; Sánchez, F.; Fontcuberta, J. Surface Symmetry-breaking and Strain Effects on Orbital Occupancy in Transition Metal Perovskite Epitaxial Films. *Nat. Commun.* **2012**, *3*, 1189.
(20) Yi, D.; Liu, J.; Okamoto, S.; Jagannatha, S.; Chen, Y.-C.; Yu, P.; Chu, Y. H.; Arenholz, E.; Ramesh, R. Tuning the Competition between Ferromagnetism and Antiferromagnetism in a Half-Doped Manganite through Magnetoelectric Coupling. *Phys. Rev. Lett.* **2013**, *111*, 127601.
(21) Peng, J. J.; Song, C.; Cui, B.; Li, F.; Mao, H. J.; Wang, Y. Y.; Wang, G. Y.; Pan, F. Exchange Bias in a Single $LaMnO_3$ Film Induced by Vertical Electronic Phase Separation. *Phys. Rev. B: Condens. Matter Mater. Phys.* **2014**, *89*, 165129.
(22) Qiao, L.; Bi, X. Direct Observation of Ni^{3+} and Ni^{2+} in Correlated $LaNiO_{3-\delta}$ Films. *Europhys. Lett.* **2011**, *93*, 57002.
(23) Soriano, L.; Preda, I.; Gutiérrez, A.; Palacín, S.; Abbate, M.; Vollmer, A. Surface Effects in the Ni 2p X-ray Photoemission Spectra of NiO. *Phys. Rev. B: Condens. Matter Mater. Phys.* **2007**, *75*, 233417.
(24) Tebano, A.; Aruta, C.; Medaglia, P. G.; Tozzi, F.; Balestrino, G. Strain-induced Phase Separation in $La_{0.7}Sr_{0.3}MnO_3$ Thin Films. *Phys. Rev. B: Condens. Matter Mater. Phys.* **2006**, *74*, 245116.
(25) Aruta, C.; Ghiringhelli, G.; Bisogni, V.; Braicovich, L.; Brookes, N. B.; Tebano, A.; Balestrino, G. Orbital Occupation, Atomic Moments, and Magnetic Ordering at Interfaces of Manganite Thin Films. *Phys. Rev. B: Condens. Matter Mater. Phys.* **2009**, *80*, 014431.
(26) Tebano, A.; Aruta, C.; Sanna, S.; Medaglia, P. G.; Balestrino, G.; Sidorenko, A. A.; De Renzi, R.; Ghiringhelli, G.; Braicovich, L.; Bisogni, V. Evidence of Orbital Reconstruction at Interfaces in Ultrathin $La_{0.67}Sr_{0.33}MnO_3$ Films. *Phys. Rev. Lett.* **2008**, *100*, 137401.
(27) Sreedhar, K.; Honig, J.; Darwin, M.; McElfresh, M.; Shand, P.; Xu, J.; Crooker, B.; Spalek, J. Electronic Properties of the Metallic Perovskite $LaNiO_3$: Correlated Behavior of 3d Electrons. *Phys. Rev. B: Condens. Matter Mater. Phys.* **1992**, *46*, 6382−6386.
(28) Garcia-Munoz, J.; Suaaidi, M.; Fontcuberta, J.; Rodriguez-Carvajal, J. Reduction of the Jahn-Teller Distortion at the Insulator-to-metal Transition in Mixed Valence Manganites. *Phys. Rev. B: Condens. Matter Mater. Phys.* **1997**, *55*, 34−37.
(29) Freeland, J.; Liu, J.; Kareev, M.; Gray, B.; Kim, J.; Ryan, P.; Pentcheva, R.; Chakhalian, J. Orbital Control in Strained Ultra-thin $LaNiO_3/LaAlO_3$. Superlattices. *Europhys. Lett.* **2011**, *96*, 57004.
(30) Chaloupka, J.; Khaliullin, G. Orbital Order and Possible Superconductivity in $LaNiO_3/LaMO_3$ Superlattices. *Phys. Rev. Lett.* **2008**, *100*, 016404.
(31) Ohzuku, T.; Takeda, S.; Iwanaga, M. Solid-state Redox Potentials for $Li[Me_{1/2}\ Mn_{2/3}]O_4$ (Me: 3d-transition metal) Having Spinel-framework Structures: A Series of 5 V Materials for Advanced Lithium-ion Batteries. *J. Power Sources* **1999**, *81*−*82*, 90−94.
(32) Dass, R. I.; Yan, J.-Q.; Goodenough, J. B. Oxygen Stoichiometry, Ferromagnetism, and Transport Properties of $La_{2-x}NiMnO_{6+\delta}$. *Phys. Rev. B: Condens. Matter Mater. Phys.* **2003**, *68*, 064415.
(33) Liu, Z. Q.; Ming, Y.; Lü, W. M.; Huang, Z.; Wang, X.; Zhang, B. M.; Li, C. J.; Gopinadhan, K.; Zeng, S. W.; Annadi, A.; Feng, Y. P.; Venkatesan, T.; Ariando. Tailoring the Electronic Properties of $SrRuO_3$ Films in $SrRuO_3/LaAlO_3$ Superlattices. *Appl. Phys. Lett.* **2012**, *101*, 223105.
(34) Ning, X. K.; Wang, Z. J.; Zhang, Z. D. Fermi Level Shifting, Charge Transfer and Induced Magnetic Coupling at $La_{0.7}Ca_{0.3}MnO_3/LaNiO_3$ Interface. *Sci. Rep.* **2015**, *5*, 8460.
(35) Aruta, C.; Ghiringhelli, G.; Tebano, A.; Boggio, N. G.; Brookes, N. B.; Medaglia, P. G.; Balestrino, G. Strain Induced X-ray Absorption Linear Dichroism in $La_{0.7}Sr_{0.3}MnO_3$ Thin Films. *Phys. Rev. B: Condens. Matter Mater. Phys.* **2006**, *73*, 235121.
(36) Chakhalian, J.; Freeland, J. W.; Habermeier, H.-U.; Cristiani, G.; Khaliullin, G.; van Veenendaal, M.; Keimer, B. Orbital Reconstruction and Covalent Bonding at an Oxide Interface. *Science* **2007**, *318*, 1114−1117.
(37) Cui, B.; Song, C.; Wang, G. Y.; Mao, H. J.; Zeng, F.; Pan, F. Strain Engineering Induced Interfacial Self-assembly and Intrinsic Exchange Bias in a Manganites Perovskite Film. *Sci. Rep.* **2013**, *3*, 2542.
(38) Chen, H. H.; Qiao, Q.; Marshall, M. S. J.; Georgescu, A. B.; Gulec, A.; Phillips, P. J.; Klie, R. F.; Walker, F. J.; Ahn, C. H.; Ismail-Beigi, S. Reversible Modulation of Orbital Occupations via an Interface-Induced Polar State in Metallic Manganites. *Nano Lett.* **2014**, *14*, 4965−4970.
(39) Scherwitzl, R.; Zubko, P.; Lichtensteiger, C.; Triscone, J.-M. Electric-field Tuning of the Metal-insulator Transition in Ultrathin Films of $LaNiO_3$. *Appl. Phys. Lett.* **2009**, *95*, 222114.
(40) Leighton, C.; Nogués, J.; Jönsson-Åkerman, B. J.; Schuller, I. K. Coercivity Enhancement in Exchange Biased Systems Driven by Interfacial Magnetic Frustration. *Phys. Rev. Lett.* **2000**, *84*, 3466−3469.
(41) Ding, J. F.; Lebedev, O. I.; Turner, S.; Tian, Y. F.; Hu, W. J.; Seo, J. W.; Panagopoulos, C.; Prellier, W.; Van Tendeloo, G.; Wu, T. Interfacial Spin Glass State and Exchange Bias in Manganites Bilayers with Competing Magnetic Orders. *Phys. Rev. B: Condens. Matter Mater. Phys.* **2013**, *87*, 054428.
(42) Huang, W. G.; Zhang, X. Q.; Du, H. F.; Yang, R. F.; Tang, Y. K.; Sun, Y.; Cheng, Z. H. Intrinsic Exchange Bias Effect in Phase-separated $La_{0.82}Sr_{0.18}CoO_3$ Single Crystal. *J. Phys.: Condens. Matter* **2008**, *20*, 445209.
(43) Binder, K.; Young, A. P. Spin glasses: Experimental Facts, Theoretical Concepts, and Open Questions. *Rev. Mod. Phys.* **1986**, *58*, 801−976.
(44) Moriga, T.; Usaka, O.; Nakabayashi, I.; Kinouchi, T.; Kikkawa, S.; Kanamaru, F. Characterization of Oxygen-deficient Phases Appearing in Reduction of the Perovskite-type $LaNiO_3$ to $La_2Ni_2O_5$. *Solid State Ionics* **1995**, *79*, 252−255.

DOI: 10.1021/acsami.5b04994
ACS Appl. Mater. Interfaces 2015, 7, 17700−17706